Mon. Not. R. Astron. Soc. **000**, 1–13 (2009) Printed 13 July 2009 (MN LATEX style file v2.2)

Cross-correlation Study between the Cosmological 21-cm Signal and the kinetic Sunyaev-Zel'dovich effect

Vibor Jelić[1⋆], Saleem Zaroubi[1], Nabila Aghanim[2], Marian Douspis[2], Léon V. E. Koopmans[1], Mathieu Langer[2], Garrelt Mellema[3], Hiroyuki Tashiro[2], Rajat M. Thomas[1,4]

[1] *Kapteyn Astronomical Institute, University of Groningen, P.O. Box 800, 9700 AV Groningen, the Netherlands*

[2] *Institut d'Astrophysique Spatiale (IAS), Bâtiment 121, F-91405, Orsay, France; Université Paris-Sud XI and CNRS (UMR 8617), France*

[3] *Stockholm Observatory, AlbaNova University Center, Stockholm University, SE-106 91, Stockholm, Sweden*

[4] *Institute for the Mathematics and Physics of the Universe (IPMU), The University of Tokyo, Chiba 277-8582, Japan*

13 July 2009

ABSTRACT

The Universe's Epoch of Reionization (EoR) can be studied using a number of observational probes that provide complementary or corroborating information. Each of these probes suffers from its own systematic and statistical uncertainties. It is therefore useful to consider the mutual information that these data sets contain. In this paper we present a cross-correlation study between the kinetic Sunyaev-Zel'dovich effect (kSZ) – produced by the scattering of CMB photons off free electrons produced during the reionization process – and the cosmological 21 cm signal – which reflects the neutral hydrogen content of the Universe, as a function of redshift. The study is carried out using a simulated reionization history in $100\ h^{-1}\ \mathrm{Mpc}$ scale N-body simulations with radiative transfer. In essence we find that the two probes anti-correlate. The significance of the anti-correlation signal depends on the extent of the reionization process, wherein extended histories result in a much stronger signal compared to instantaneous cases. Unfortunately however, once the primary CMB fluctuations are included into our simulation they serve as a source of large correlated noise that renders the cross-correlation signal insignificant, regardless of the reionization scenario.

Key words: cosmology: theory, cosmic microwave background, large scale structure of universe, diffuse radiation, radio lines: general

1 INTRODUCTION

The Epoch of Reionization (EoR) is one of the least explored periods in the history of the Universe. At present, there are only a few tentative observational constrains on the EoR like the Gunn-Peterson troughs (Gunn & Peterson 1965; Fan et al. 2006) and the cosmic microwave background (CMB) E-mode polarization (Page et al. 2007) at large scales. Both of these observations provide strong yet limited constraints on the EoR. In the near future, however, a number of observations at various wavelengths (e.g., redshifted 21 cm from HI, Lyman-α emitters, high redshift QSOs, etc.) are expected to probe this pivotal epoch in much greater detail. Among these, the cosmological 21 cm transition line of neutral hydrogen is the most promising probe of the intergalactic medium (IGM) during reionization (Madau et al. 1997)

A number of radio telescopes (e.g. LOFAR[1], MWA[2], and SKA[3]) are currently being constructed/designed that aim at detecting the redshifted 21 cm line to study the EoR. Unfortunately, these experiments will suffer from a high degree of contamination, due both to astrophysical interlopers like the Galactic and extra-galactic foregrounds and non-astrophysical instrumental effects (e.g. Jelić et al. 2008; Labropoulos et al. 2009). Fortunately, the signal has some characteristics which differentiates it from the foregrounds and noise, and using proper statistics may extract signatures of reionization (e.g. Furlanetto et al. 2004; Harker et al. 2009b,a). In order to reliably detect the cosmological signal from the observed data, it is essential to understand in detail all aspects of the data and their influence on the extracted signal.

Given the challenges and uncertainities involved in measuring the redshifted 21-cm signal from the EoR, it is vital to corroborate this result with other probes of the EoR. In this paper we study the information imprinted on the CMB by the EoR and its cross correlation with the 21 cm probe. Given the launch of the recent PLANCK satellite, that will measure the CMB with unprecented accuracy, it is only fitting to conduct a rigorous study into the cross-correlation of these data sets.

One of the leading sources of secondary anisotropy in the CMB is due to the scattering of CMB photons off free electrons, created during the reionization process, along the line of sight

⋆ E-mail: vjelic@astro.rug.nl

[1] http://www.lofar.org

[2] http://www.haystack.mit.edu/ast/arrays/mwa

[3] http://www.skatelescope.org

(LOS) (Zeldovich & Sunyaev 1969). These anisotropies when induced by thermal motions of free electrons is called the thermal Sunyaev-Zel'dovich effect (tSZ) and whence due to bulk motion of free electrons, the kinetic Sunyaev-Zel'dovich effect (kSZ). The latter is far more dominant during reionization (for a review of secondary CMB effects see Aghanim et al. 2008).

The kSZ effect from a homogeneously ionized medium, i.e., with ionized fraction only a function of redshift, has been studied both analytically and numerically by a number of authors; the linear regime of this effect first calculated by Sunyaev & Zeldovich (1970) and subsequently revisited by Ostriker & Vishniac (1986) and Vishniac (1987) – hence also referred to as the Ostriker-Vishniac (OV) effect. In recent years various groups have calculated this effect in its non-linear regime using semi-analytical models and numerical simulations (Gnedin & Jaffe 2001; Santos et al. 2003; Zhang et al. 2004). These studies show the contribution due to non-linear effects being important only at small angular scales ($l > 1000$), while the OV effect dominate at large angular scales.

The kSZ effect from patchy reionization was first estimated using simplified semi-analytical models (Santos et al. 2003) wherein they concluded that fluctuations caused by patchy reionization dominate over anisotropies induced by homogeneous reionization. However, for a complete picture of the CMB anisotropies induced by the EoR a more detailed modeling is required. Over and above the underlying density and velocity fields these details should include the formation history and "nature" of the first ionizing sources and the radiative transport of ionizing photons to derive the reionization history (sizes and distribution of the ionized bubbles). Some recent numerical simulations of the kSZ effect during the EoR were carried out by Salvaterra et al. (2005); Zahn et al. (2005); Doré et al. (2007); Iliev et al. (2007).

Cross-correlation between the cosmological 21 cm signal and the secondary CMB anisotropies provide a potentially useful statistic. The cross-correlation has the advantage that the measured statistic is less sensitive to contaminants such as the foregrounds, systematics and noise, in comparison to "auto-correlation" studies. Analytical cross-correlation studies between the CMB temperature anisotropies and the EoR signal on large scales ($l \sim 100$) have been carried out by Alvarez et al. (2006); Adshead & Furlanetto (2008) and on small scales ($l > 1000$) by Cooray (2004); Salvaterra et al. (2005); Slosar et al. (2007). Thus far the only numerical study of the cross-correlation has been carried out by Salvaterra et al. (2005). Some additional analytical work on cross-correlation between the E- and B-modes of CMB polarization with the redshifted 21 cm signal have been done by Tashiro et al. (2008); Dvorkin et al. (2009).

In this paper we first calculate the kSZ anisotropies from the homogeneous and patchy reionization based on $100\,h^{-1}\,\mathrm{Mpc}$ scale numerical simulations of reionization. We then cross-correlate them with the expected EoR maps obtained via the same simulations, and we discuss how the large-scale velocites and primary CMB fluctuations influence the cross-correlation. Although similar in some aspects, the work presented here differ from Salvaterra et al. (2005) substantially. First, Salvaterra et al. used a relatively small computational box ($20\,h^{-1}\,\mathrm{Mpc}$) incapable of capturing relevant large-scale density and velocity pertubations. Secondly, the primary CMB fluctuation, that manifests itself as a large background noise, is not taken into the cross-correlation study. And finally, there is a difference in procedure for calculating that cross-correlation coefficient.

The paper is organized as follows. In Section 2 we discuss kSZ signal and cosmological 21 cm signal from the EoR. In Section 3 we present the numerical simulations employed to obtain the kSZ and EoR maps for a specifc reionization history. Cross-correlation between the cosmological 21 cm fluctuations (EoR signal) and the kSZ anisotropies, together with the influence of the large-scale velocities and the primary CMB fluctuations on CMB-EoR cross-correlation are discussed in Section 4. Finally in Section 5 we present our discussions and conclusions on the topic.

Throughout we assume ΛCDM-cosmology with WMAP5 parameters (Komatsu et al. 2008): $H_0 = 71.9\ \mathrm{kms}^{-1}\mathrm{Mpc}^{-1}$, $\Omega_\mathrm{b} = 0.0441$, $\Omega_\mathrm{m} = 0.258$ and $\Omega_\Lambda = 0.742$.

2 THEORY

In the following section we briefly review the theoretical aspects of the kinetic Sunayev-Zel'dovich (kSZ) effect and the cosmological 21 cm signal from the epoch of reionization. In addition, the relevant mathematical forms used to calculate the kSZ and the cosmological 21 cm signals are presented.

2.1 Kinetic Sunayev-Zel'dovich effect

The temperature fluctuation of the CMB caused by the Thompson scattering of its photons off populations of free electrons in bulk motion, for a given line of sight (LOS), is:

$$\left(\frac{\delta T}{T}\right)_\mathrm{kSZ} = -\sigma_\mathrm{T}\int_{t_\mathrm{r}}^{t_0} \mathrm{e}^{-\tau} n_\mathrm{e}(\hat{r}\cdot\vec{v})\mathrm{d}t, \tag{1}$$

where τ is the optical depth of electrons to Thomson scattering, $\vec{v}$ the bulk velocity of free electrons and $\hat{r}$ the unit vector denoting the direction of the LOS. The integral is performed for each LOS with t_r the time at the epoch recombination and t_0 the age of the Universe today. Note that all quantities are in physical units. Temperature fluctuations produced at time t will be attenuated due to multiple scattering along the LOS to the present time and is accounted for by the $\mathrm{e}^{-\tau}$ term.

The electron density can be written as the product of the neutral atom density n_n and ionization fraction x_e. Both n_n and x_e vary about their average value $\bar{n}_\mathrm{n}$ and $\bar{x_\mathrm{e}}$ and thus these fluctuations can be defined as $\delta = n_\mathrm{n}/\bar{n}_\mathrm{n} - 1$ and $\delta_{x_\mathrm{e}} = x_\mathrm{e}/\bar{x}_\mathrm{e} - 1$ and consequently the electron density expressed as:

$$n_\mathrm{e} = \bar{n}_\mathrm{n}\bar{x}_\mathrm{e}(1 + \delta + \delta_{x_\mathrm{e}} + \delta\delta_{x_\mathrm{e}}). \tag{2}$$

In first approximation one can just follow the reionization of hydrogen and assume that the neutral atom density equals neutral hydrogen density. However, in our simulation we follow both hydrogen and helium reionization. Assuming both hydrogen and helium follow the underlying dark matter density, the neutral atom density is a sum of the neutral hydrogen (n_HI) and neutral helium (n_HeI) densities: $n_\mathrm{n} = (\bar{n}_\mathrm{HI} + \bar{n}_\mathrm{HeI})(1+\delta)$. Moreover, the electron density can be written as:

$$n_\mathrm{e} = n_\mathrm{HI}x_\mathrm{HII} + n_\mathrm{HeI}x_\mathrm{HeII} + 2n_\mathrm{HeI}x_\mathrm{HeIII}, \tag{3}$$

where $n_\mathrm{HII,HeII,HeIII}$ and $x_\mathrm{HII,HeII,HeIII}$ are densities and ionization fractions of HII, HeII and HeIII respectively. The ionization fractions are defined as: $x_\mathrm{HII} = n_\mathrm{HII}/n_\mathrm{HI}$, $x_\mathrm{HeII} = n_\mathrm{HeII}/n_\mathrm{HeI}$ and $x_\mathrm{HeIII} = n_\mathrm{HeIII}/n_\mathrm{HeI}$.

The mean hydrogen and helium densities vary with redshift as $\bar{n}_\mathrm{HI,HeI} = \bar{n}_\mathrm{HI(0),HeI(0)}(1+z)^3$, where $\bar{n}_\mathrm{HI(0),HeI(0)}$ are the mean hydrogen and helium densities at the present time: $\bar{n}_\mathrm{HI(0)} = 1.9\times10^{-7}\ \mathrm{cm}^{-3}$ and $\bar{n}_\mathrm{HeI(0)} = 1.5\times10^{-8}\ \mathrm{cm}^{-3}$.

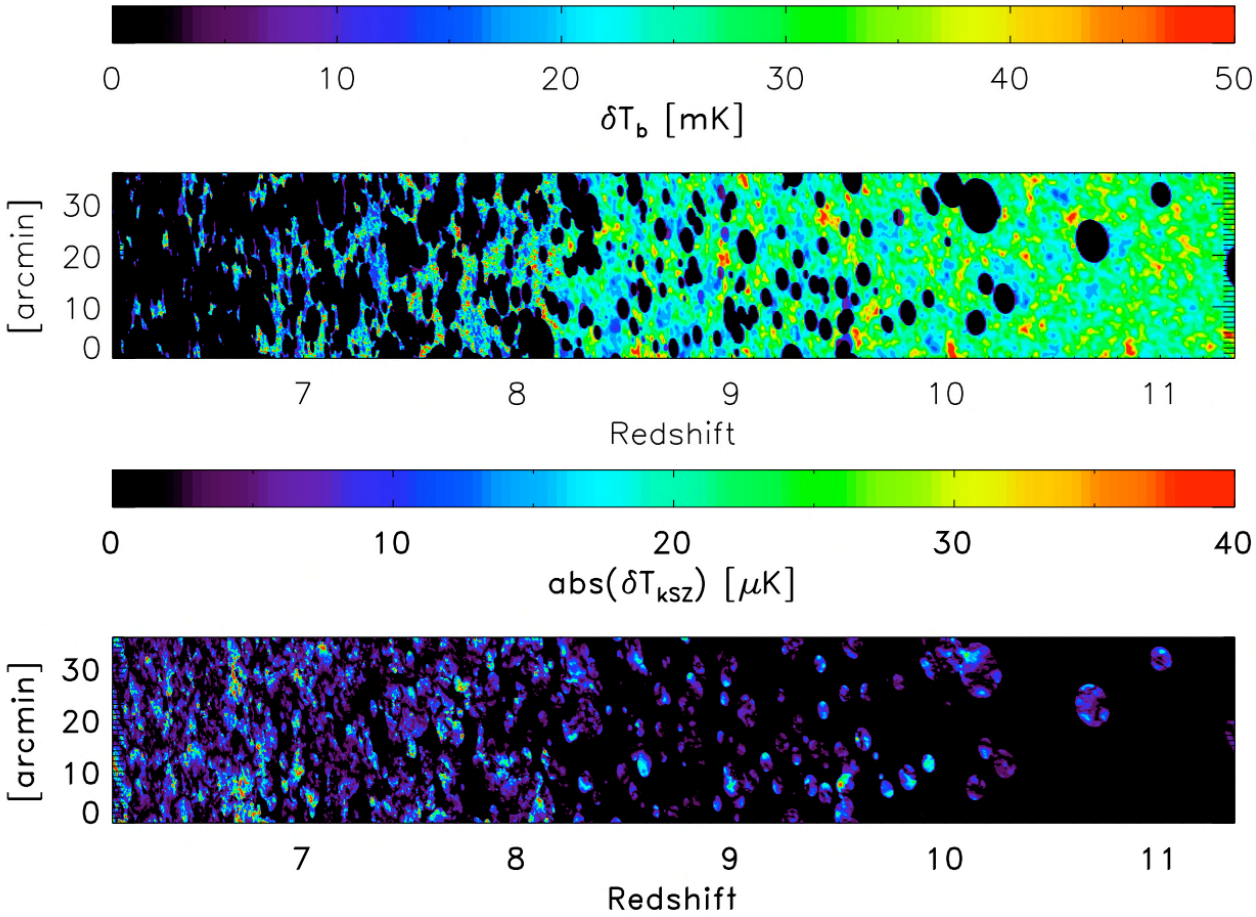

Figure 1. *A slice through the simulated redshift cube of the the cosmological 21 cm signal (top panel) and the kSZ effect (bottom panel) in the case of the 'Stars' patchy reionization model. The angular scale of the slices is* $\sim 0.6°$.

By inserting Eq. 2 into Eq. 1 and converting Eq. 1 from an integral in time to one in redshift space [4] (z), we get:

$$\left(\frac{\delta T}{T}\right)_{\rm kSZ} = -\sigma_{\rm T}\bar{\rm n}_{\rm n(0)}\int_{z_{\rm r}}^{z_0}\frac{(1+z)^2}{H}{\rm e}^{-\tau}\bar{x_e} \cdot(1+\delta+\delta_{x_e}+\delta\delta_{x_e})v_{\rm r}{\rm d}z, \quad (4)$$

where $v_{\rm r}$ is component of $\vec{v}$ along the LOS ($v_r = \hat{r}\cdot\vec{v}$) and $\bar{n}_{\rm n(0)} = \bar{n}_{\rm HI(0)} + \bar{n}_{\rm HeI(0)}$. For a ΛCDM Universe the Hubble constant at redshift z is $H = {\rm H}_0\sqrt{\Omega_{\rm m}(1+z)^3+\Omega_\Lambda}$ where ${\rm H}_0$ is the present value of the Hubble constant, $\Omega_{\rm m}$ is the matter and Ω_Λ the dark energy densities, respectively.

For homogeneous reionization histories, i.e. a uniform change in the ionization fraction as a function of redshift, Eq. 4 becomes:

$$\left(\frac{\delta T}{T}\right)_{\rm kSZ} = -\sigma_{\rm T}\bar{\rm n}_{\rm H(0)}\int_{z_{\rm r}}^{z_0}\frac{(1+z)^2}{H}{\rm e}^{-\tau}\bar{x_e}(1+\delta)v_{\rm r}{\rm d}z, \quad (5)$$

which means that the kSZ fluctuations are induced only by spatial variations of the density field. The linear regime of this effect is called the Ostriker-Vishniac (OV) effect. The OV effect is of second order and peaks at small angular scales (arc minutes) and has an rms of the order of a few μK.

[4] In order to make transformation of the Eq. 1 to the redshift space we use ${\rm d}t = -\frac{{\rm d}z}{H(z)[1+z]}$, where $H(z)$ is Hubble constant at redshift z.

2.2 The Cosmological 21 cm signal

In radio astronomy, where the Rayleigh-Jeans law is applicable, the radiation intensity, $I(\nu)$ is expressed in terms of the brightness temperature T_b:

$$I(\nu) = \frac{2\nu^2}{c^2}kT_b, \quad (6)$$

where ν is the frequency, c is the speed of light and k is Boltzmann's constant. The predicted differential brightness temperature of the cosmological 21 cm signal with the CMB as the background is given by (Field 1958, 1959; Ciardi & Madau 2003):

$$\delta T_{\rm b} = 26\ {\rm mK}\ x_{\rm HI}(1+\delta)\left(1-\frac{T_{\rm CMB}}{T_{\rm s}}\right)\left(\frac{\Omega_{\rm b}h^2}{0.02}\right)\left[\left(\frac{1+z}{10}\right)\left(\frac{0.3}{\Omega_{\rm m}}\right)\right]^{1/2}. \quad (7)$$

Here $T_{\rm s}$ is the spin temperature, $x_{\rm HI}$ is the neutral hydrogen fraction, δ is the matter density contrast and $h = H_0/(100\ {\rm kms}^{-1}{\rm Mpc}^{-1})$. If we express the neutral hydrogen fraction as $x_{\rm HI} = \bar{x}_{\rm HI}(1+\delta_{x_{\rm HI}})$, Eq. 7 becomes:

$$\delta T_{\rm b} = 26\ {\rm mK}\ \bar{x}_{\rm HI}(1+\delta+\delta_{x_{\rm HI}}+\delta\delta_{x_{\rm HI}})\left(1-\frac{T_{\rm CMB}}{T_{\rm s}}\right)\left(\frac{\Omega_{\rm b}h^2}{0.02}\right)\left[\left(\frac{1+z}{10}\right)\left(\frac{0.3}{\Omega_{\rm m}}\right)\right]^{1/2}. \quad (8)$$

In his two seminal papers, Field (1958, 1959) calculated the spin temperature, T_s, as a weighted average of the CMB, kinetic and colour temperatures:

$$T_s = \frac{T_{CMB} + y_{kin}T_{kin} + y_\alpha T_\alpha}{1 + y_{kin} + y_\alpha}, \quad (9)$$

where T_{CMB} is the CMB temperature and y_{kin} and y_α are the kinetic and Lyman-α coupling terms, respectively. We have assumed that the color temperature, T_α, is equal to T_{kin} (Madau et al. 1997). The kinetic coupling term increases with the kinetic temperature, whereas the y_α coupling term depends on Lyman-α pumping through the so-called Wouthuysen-Field effect (Wouthuysen 1952; Field 1958). The two coupling terms are dominant under different conditions and in principle could be used to distinguish between ionization sources, e.g., between first stars, for which Lyman-α pumping is dominant, vs. first mini-quasars for which X-ray photons and therefore heating is dominant (see e.g., Madau et al. 1997; Zaroubi et al. 2007; Thomas & Zaroubi 2008).

3 SIMULATIONS

The kSZ ($\delta T/T$) and the cosmological 21 cm maps (δT_b) are simulated using the following data cubes: density (δ), radial velocity (v_r) and HI, HII, HeI, HeII and HeIII fractions ($x_{\rm HI,HII,HeI,HeII\&HeIII}$). The data cubes are produced using the BEARS algorithm, a fast algorithm to simulate the EoR signal (Thomas et al. 2009).

In the following subsections we summarize the BEARS algorithm and describe operations done on the output in order to calculate the kSZ and the EoR maps. Furthermore, we detail the calculations to obtain the optical depth and kSZ signal along a certain LOS. Finally we present the maps of the kSZ temperature fluctuations for the two patchy reionization models ('stars' and 'mini-quasars') and discuss aspects of their contribution to the signal.

3.1 BEARS algorithm: overview

BEARS is a fast algorithm to simulate the underlying cosmological 21 cm signal from the EoR. It is implemented by using an N-body/SPH simulation in conjunction with a 1-D radiative transfer code under the assumption of spherical symmetry of the ionized bubbles. The basic steps of the algorithm are as follows: first, a catalogue of 1D ionization profiles of all atomic hydrogen and helium species and the temperature profile that surround the source is calculated for different types of ionizing sources with varying masses, luminosities at different redshifts. Subsequently, photon rates emanating from dark matter haloes, identified in the N-body simulation, are calculated semi–analytically. Finally, given the spectrum, luminosity and the density around the source, a spherical ionization bubble is embedded around the source, whose radial profile is selected from the catalogue as generated above. For more details refer Thomas et al. (2009).

As outputs we obtain data cubes (2D slices along the frequency/redshift direction) of density (δ), radial velocity (v_r) and hydrogen and helium fractions ($x_{\rm HI,HII,HeI,HeII\&HeIII}$). Each data cube consists of about 850 slices each representing a certain redshift between 6 and 11.5. Slices have a size of $100\ {\rm h}^{-1}$ comoving Mpc and are defined on a 512^2 grid. Becauses these slices are produced to simulate a mock dataset for radio-interferometric experiments, they are uniformly spaced in frequency (therefore, not uniform in redshift). Thus, the frequency resolution of the instrument dictates the scales over which structures in the Universe are averaged/smoothed along the redshift direction. The relation between frequency ν and redshift space z is given by:

$$z = \frac{\nu_{21}}{\nu} - 1, \quad (10)$$

where $\nu_{21} = 1420$ MHz is the rest frequency that corresponds to the 21cm line.

The final data cubes are produced using approximately 35 snapshots of the cosmological simulations. Since choice of the redshift direction in each box is arbitrary, three final data cubes can be produced in this manner (x, y and z).

3.2 Randomization of the structures

The kSZ effect is an integrated effect and is sensitive to the structure distribution along the LOS. To avoid unnatural amplification of the kSZ fluctuations due to repeating structures in the simulated data cubes, we follow Iliev et al. (2007) and introduce randomization of the structures along the LOS over $100\ {\rm Mpc/h}$ scale in two steps. First, each $100\ {\rm Mpc/h}$ chunk of the data cube is randomly shifted (assuming periodic boundary conditions) and rotated in a direction perpendicular to the LOS. The shift can be positive or negative in any direction (x and(or) y) by an integer value between 0 and 512. While the rotation can be clockwise or anticlockwise by an $n\pi/2$ angle (n=0,1,2,3). Secondly the final data cube is produced by assembling the first $100\ {\rm Mpc/h}$ part from the x-data cube, second from the y-data cube, third from the z-data cube and then back to the x-data cube and so on., to a distance that spans the comoving radial distance between redshifts 6 and 12.

3.3 Optical depth

Thomson optical depth τ at redshift z is:

$$\tau = {\rm c}\sigma_{\rm T} \int_0^z n_{\rm e} \frac{(1+z)^2}{H(z)} {\rm d}z, \quad (11)$$

where ${\rm c} = 2.998 \times 10^8\ {\rm m\,s^{-1}}$ is the speed of light, $\sigma_{\rm T} = 6.65 \times 10^{-29}\ {\rm m^2}$ the Thomson scattering cross section for electrons, $n_{\rm e}$ the density of free electrons and $H(z)$ the Hubble constant at redshift z.

In our simulations we split the integral into two parts. The first part that represents the mean Thomson optical depth ($\bar{\tau}_{06}$) between the redshift 0–6 and the second, τ_{6z}, from redshift 6 to a desired redshift z. This choice is driven by the limited redshift range ($z \sim 6 - 11.5$) of imminent radio astronomical projects designed to map the EoR. Under the assumption that the reionization is completed by the redshift 6, the mean Thomson optical depth $\bar{\tau}_{06}$ is 0.0517. Note that our simulation is set to have a mean Thomson optical depth of 0.087, as obtained from the CMB data ($\tau = 0.087 \pm 0.017$, Komatsu et al. (2008)).

3.4 Creating the kSZ and EoR maps

For clarity we summarize the steps we follow to create the kSZ and EoR maps for a given scenario of the reionization history:

(i) Using the output of BEARS, data cubes for the density, radial velocity, helium and hydrogen fractions are produced.

(ii) Data cubes are randomized over $100\ {\rm Mpc/h}$ scale along the redshift direction.

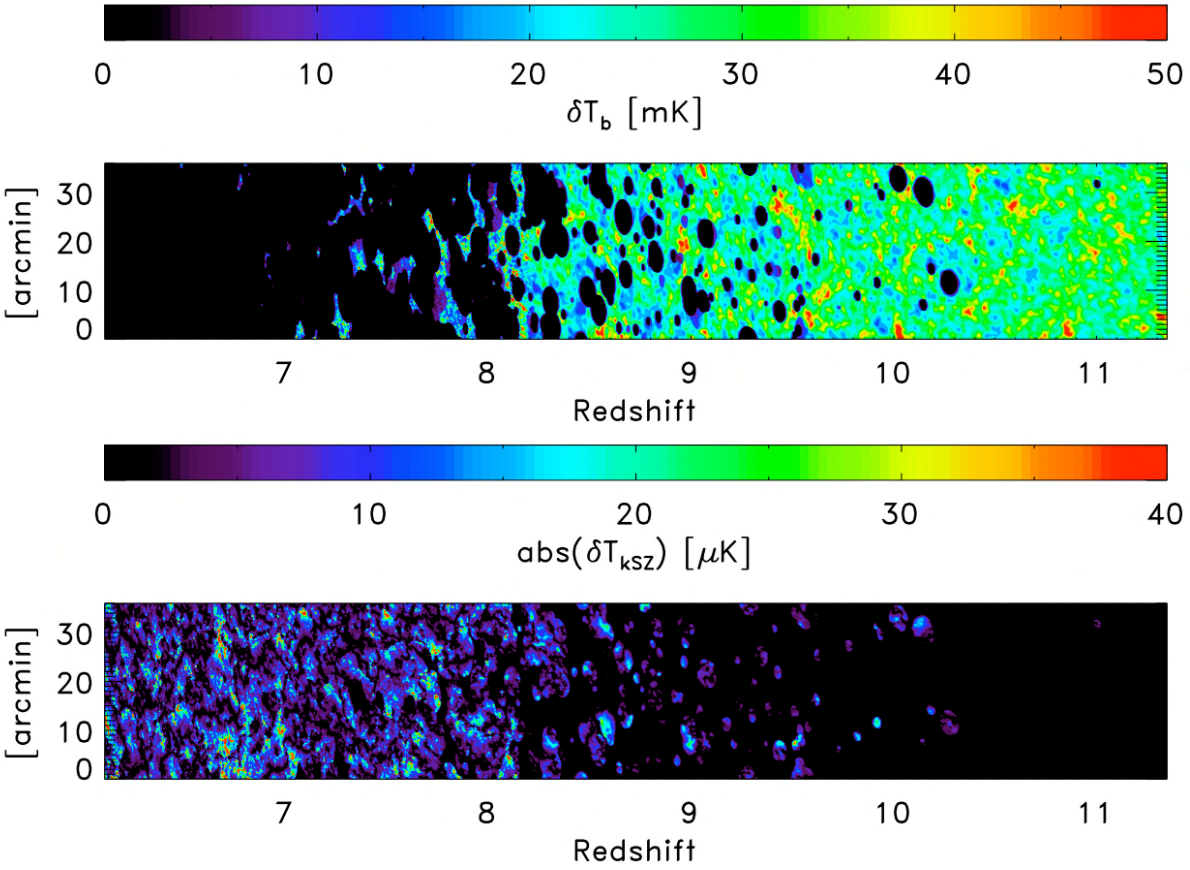

Figure 2. *The same as a Fig. 2 but for the 'QSOs' patchy reionization model.*

(iii) Using Eq. 11 the Thomson optical depth, τ, is calculated to a redshift z.

(iv) Using the integrand of the Eq. 4, data cubes with the kSZ signal is produced as a function of redshift.

(v) Integrating along each LOS through the kSZ data cube the integrated kSZ map is obtained. Note that we assume that the reionization is complete by redshift 6, so the integral in Eq. 4 spans $z > 6$.

(vi) Finally, the brightness temperature fluctuations, δT_b, is calculated using Eq. 8.

In the following sections we will use the kSZ and EoR maps produced for three different models of reionization:

(i) HOMOGENEOUS: Reionization history is homogeneous and ionized fraction follows:

$$x_e = \frac{1}{1 + e^{k(z - z_{\rm reion})}}, \qquad (12)$$

with $z_{\rm reion}$ set to 8.5 and $k = 1, 2, ...$ tunes the "rapidness" of the reionization process.

(ii) PATCHY STARS: Reionization history is patchy, gradual and extended with stars as the sources of ionization.

(iii) PATCHY QSOS: Reionization history is patchy and relatively fast with QSOs as the ionizing sources.

Fig. 1 & Fig. 2 show slices through the simulated redshift cube of the cosmological 21 cm signal ($\delta T_{\rm b}$) and the kSZ effect ($\delta T_{\rm kSZ}$) in the case of 'Stars' and 'QSOs' patchy reionization models. The angular size of the slices is $\sim 0.6^{\circ}$.

Apart from the difference in the global shape of the reionization histories driven by 'Stars' and 'QSOs' (see Fig. 4), the average size of the ionization bubble is also smaller in 'Stars' compared to that of 'QSOs'. For a detailed description and comparison of reionization histories due to 'Stars' and 'QSOs' see Thomas et al. (2009).

The kSZ anisotropies from patchy reionization is induced by both fluctuations of the density field δ and ionization fraction $\delta_{x_{\rm e}}$ (see Eq. 4). Santos et al. (2003) found that kSZ anisotropies from $\delta_{x_{\rm e}}$ fluctuations dominate over δ modulated fluctuations (OV effect). In order to test this result with our simulations we split the integral in Eq. 4 into three parts and produce three integrated kSZ maps (for the 'Stars' model see Fig. 3). The first term '$1+\delta$' represents the density induced secondary anisotropies (OV effect). The '$\delta_{x_{\rm e}}$' term represents the secondary anisotropies due to patchiness in the reionization and '$\delta\delta_{x_{\rm e}}$' represents a higher order anisotropy.

The $mean$ and rms of the '$1 + \delta$', '$\delta_{x_{\rm e}}$' and '$\delta\delta_{x_{\rm e}}$' components of the simulated kSZ maps are shown in the Table 1 for patchy reionization in the 'Stars' and 'QSOs' model. The rms value of the maps is used as a measure of the fluctuations. We confirm that the '$\delta_{x_{\rm e}}$' fluctuations are indeed larger than density induced anisotropies ('δ') for both patchy reionization models. However the difference between the '$\delta_{x_{\rm e}}$' and 'δ' fluctuations is much larger for the 'Stars'reionization history model than 'QSOs' model. Also note that the third order anisotropy ('$\delta\delta_{x_{\rm e}}$') is not negligible in both reionization scenarios. For completeness we also show contribution from the pure Doppler term ('1') in Eq. 4.

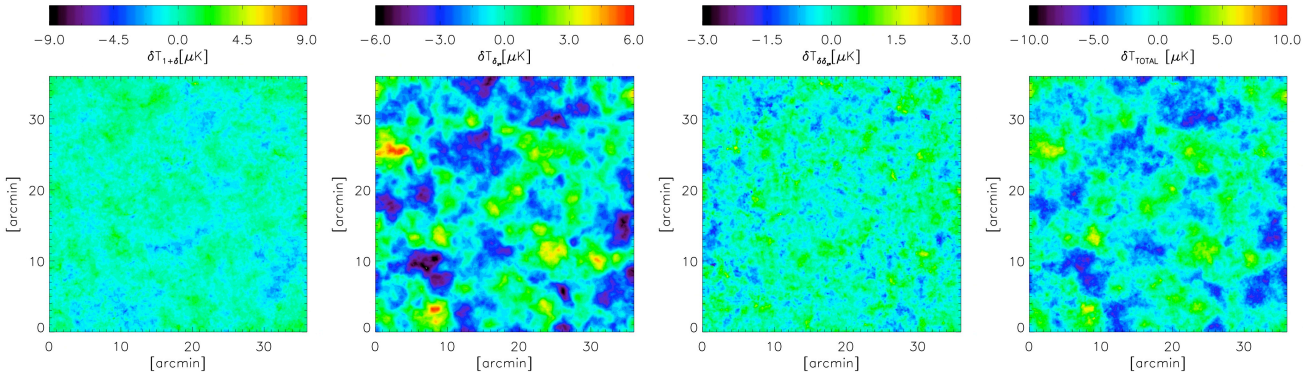

Figure 3. *The simulated kSZ anisotropies induced by '$1+\delta$' (first panel), 'δ_{x_e}' (second panel) and '$\delta\delta_{x_e}$' term (third panel) in Eq. 4 for patchy reionization model by 'Stars'. The kSZ anisotropies induced by all terms together in Eq. 4 are showed on fourth panel ('*TOTAL*'). The* mean *and* rms *of the simulated kSZ maps is shown in Table 1. Note that each map has its own color scale.*

Table 1. The $mean$ and rms of the '$1+\delta$', 'δ_{x_e}' and '$\delta\delta_{x_e}$' simulated kSZ maps for both 'Stars' (see Fig. 3) and 'QSOs' patchy reionization model. C_0 is a cross-correlation coefficent at a zero lag between coresponding kSZ maps and integrated EoR map (see Section 4). For completeness we also show results for the pure Doppler term ('1') in Eq. 4.

	$\delta T_{\rm kSZ}$	'1'	'$1+\delta$'	'δ_{x_e}'	'$\delta\delta_{x_e}$'	TOTAL
STARS	$mean$ [μK]	-0.004	0.03	0.58	0.02	0.63
	rms [μK]	0.14	0.80	1.74	0.40	2.00
	C_0	0.05	-0.003	-0.12	-0.06	-0.11
QSOS	$mean$ [μK]	-0.002	0.03	0.27	0.01	0.30
	rms [μK]	0.15	0.93	1.28	0.28	1.57
	C_0	0.1	0.04	-0.08	-0.01	-0.06

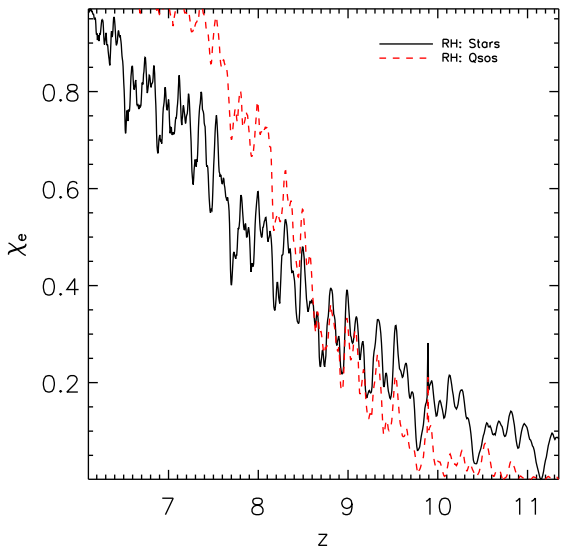

Figure 4. *The mean ionization fraction x_e as a function of redshift for the 'Stars' and 'QSOs' patchy reionization model.*

4 CROSS-CORRELATION KSZ-EOR MAPS

The kSZ effect from the EoR is expected to be correlated with cosmological 21 cm maps for a homogeneous reionization history and anti-correlated when patchy (Cooray 2004; Salvaterra et al. 2005; Alvarez et al. 2006; Slosar et al. 2007; Adshead & Furlanetto 2008). In this section simulations described in Section 3 are used to explore the small angular scale cross-correlation between the kSZ effect and EoR maps for five different reionization histories. Further, we will fold-in the influence of i) the large-scale velocities on the kSZ effect and ii) the primary CMB fluctuations on the cross-correlation.

Throughout the paper we will use a normalized cross-correlation in order to be able to compare results from a different pairs of maps. The normalized cross-correlation between two images ($a_{i,j}$ and $b_{i,j}$) with the same total number of pixels n is defined at zero lag as:

$$C_0 = \frac{1}{n-1}\sum_{i,j}\frac{(a_{i,j}-\bar{a})(b_{i,j}-\bar{b})}{\sigma_a\sigma_b}, \qquad (13)$$

where $\bar{a}$ ($\bar{b}$) is the mean and σ_a (σ_b) the standard deviation of the image a (b). However, the cross-correlation between the kSZ and the EoR map needs to be considered more carefully.

The fluctuations of the kSZ effect over the simulated map are both positive and negative, since the radial velocity v_r can be both positive and negative (see Eq. 4). In contrast, the EoR signal fluctuations in our simulations are always positive (see Eq. 8). When calculating the cross-correlation between these two maps, we are interested in finding the number of points at which both signals are present (homogeneous reionization model) or where one signal is present and the other absent (patchy reionization model). In other words only the absolute value of the kSZ fluctuation is relevant in our calculation and not its sign.

4.1 Homogeneous reionization history

We explore the cross-correlation between the kSZ map and integrated EoR map in the case of three different homogeneous reionization histories (HRH1, HRH2 & HRH3). These histories are modulated by Eq. 12, with k controlling the duration of reionization. The mean ionization fraction $x_e(z)$ for these models are shown in Fig. 5.

The cross correlation between an integrated kSZ map and an

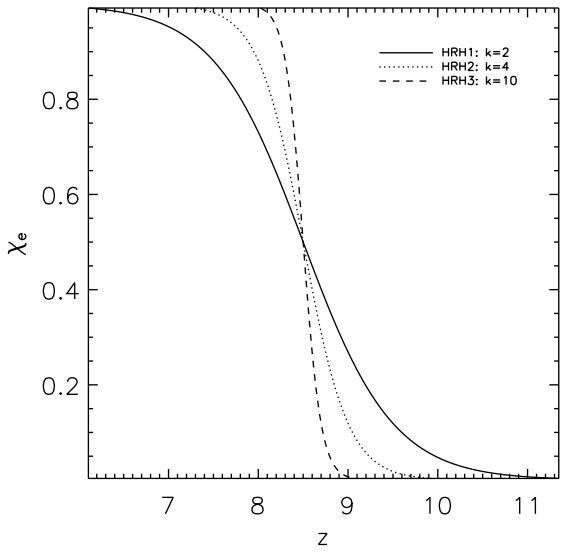

Figure 5. *The ionization fraction x_e as a function of redshift for three different models of the homogeneous reionization history (*HRH 1*,* HRH 2 *&* HRH 3*). All three models are defined by Eq. 12 but have different values of k (different reionization durations). The half of the reionization process is set in all three models to $z_{reion} = 8.5$.*

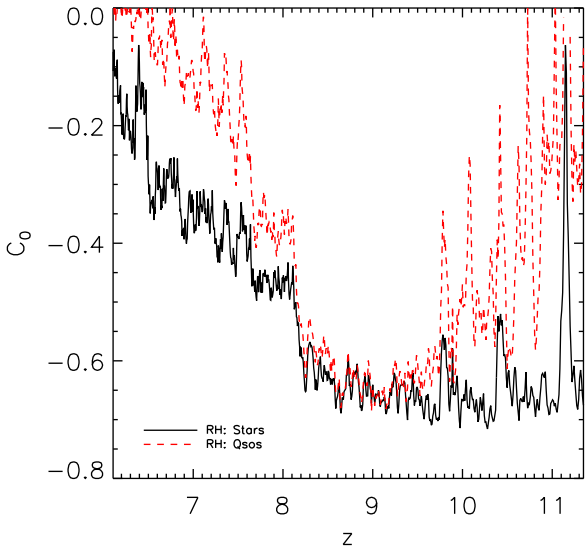

Figure 6. *The zero lag cross-correlation coefficient (C_0) between the kSZ map and the EoR map at a given redshift. The solid black line corresponds to the 'Stars' while the dashed red line the 'QSOs' patch reionization model. For both reionization models we find an anti-correlation between the maps.*

integrated EoR map results in a coefficient $C_{0,\text{HRH 1}} = 0.10 \pm 0.03$ for an extended homogeneous reionization history (HRH 1). For HRH 2 $C_{0,\text{HRH 2}} = 0.21 \pm 0.02$ and HRH 3 $C_{0,\text{HRH 3}} = 0.24 \pm 0.02$. The errors are estimated by performing a Monte Carlo calculation with 200 independent realizations of the integrated kSZ and EoR maps using the randomization procedure explained in Section 3.

As expected, the integrated kSZ and EoR maps are correlated for homogeneous models of reionization. Furthermore, the correlation depends on the duration of reionization with larger values for more 'rapid' reionization. These results are in agreement with Alvarez et al. (2006).

4.2 Patchy reionization history

For patchy reionization models we first cross-correlate the kSZ and the EoR map at a given redshift. The resulting zero lag coefficient (C_0), as a function of redshift, is shown in Fig. 6. The solid black line represents the correlation for 'Stars' while the dashed red line the 'QSOs' patchy reionization model. As expected for patchy reionization in both models, the kSZ and the EoR map anti-correlate at individual redshifts.

Note that Eq. 13 is not taking into account a statistical weight (significance) of the result. The statistical weight can be defined with a factor $2n_*/n$ where n_* represents the number of $a_{i,j} \cdot b_{i,j}$ products that are non-zero. This makes the result the most significant when both signals are represented equally and less significant when one signal is present and the other not.

The obtained anti-correlation is also evident by visual inspection of the kSZ and EoR slices through the simulated redshift cubes (see Fig. 1 & 2). One can see that the kSZ signal is present only at the regions where the EoR signal is not. This result is not surprising since the EoR signal is proportional to neutral hydrogen while the kSZ to the ionized, both of which are almost mutually exclusive.

In reality, we are not able to measure the kSZ effect at a certain redshift but only an integrated effect along the entire history. Thus we can only cross-correlate the integrated kSZ map with the integrated EoR map and/or the EoR maps at different redshifts [5].

Fig. 7 shows the integrated EoR and kSZ map for the 'Stars' (first two panels) and 'QSOs' (last two panels) patchy reionization model . The cross-correlation coefficient at zero lag for these two models are $C_{0,\text{Stars}} = -0.17$ and $C_{0,\text{QSOs}} = -0.02$. In order to determine the error on the kSZ-EoR cross-correlation, we perform a Monte Carlo calculation. After creating 200 independent realizations of the integrated kSZ and EoR maps using the randomization procedure explained in Section 3, we calculate the cross-correlation coefficient for each pair of realizations. Finally, we calculate the mean and standard deviation of the cross-correlations. For the 'Stars' model we get $C_{0,\text{Stars}} = -0.16 \pm 0.02$, while for the 'QSOs' model $C_{0,\text{QSOs}} = -0.05 \pm 0.02$.

To understand higher values of the cross-correlation coefficient in 'Stars' compared to the 'QSOs' model, one needs analyze Fig. 4 and Table 1. It is evident from Fig. 4 that the reionization history is gradual and extended with stars as ionizing sources, compared to a shorter and sharper history with QSOs as ionizing sources. Moreover, the patchy term ('δ_{x_e}') of the kSZ fluctuations is much larger than the homogeneous component in the anisotropy ('δ') in the case of 'Stars' than for 'QSOs' model (see Table 1). We showed beforehand that the kSZ effect correlates with the cosmological 21 cm signal for homogeneous reionization and that the correlation is strongest for an 'instant' reionization history. We also obtain the same result by correlating different kSZ components with the integrated EoR map (see Table 1). Combining these results we see the cross-correlation is driven by the patchy kSZ anisotropies in the 'Stars' model, while in the 'QSOs' model the homogeneous and patchy kSZ anisotropies tend to cancel each

[5] This is because, unlike the kSZ effect, we can potentially obtain redshift-specific information of neutral hydrogen via upcoming radio telescopes.

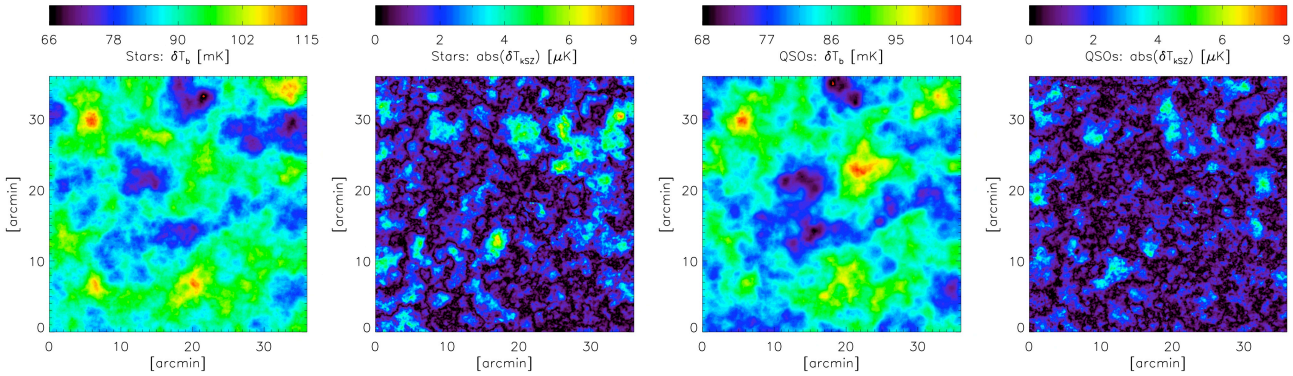

Figure 7. *The integrated EoR and kSZ map for the 'Stars' (first two panels) and 'QSOs' patchy reionization model (second two panels). The mean cross-correlation coefficient at the zero lag between integrated EoR map and integrated kSZ map is* $C_{0,\mathrm{Stars}} = -0.16 \pm 0.02$ *for the 'Stars' and* $C_{0,\mathrm{QSOs}} = -0.05 \pm 0.02$ *for the 'QSOs' model.*

other. As a consequence, the anti-correlation in 'QSOs' model is much weaker than that of 'Stars'.

In addition to the balance between homogeneous and patchy kSZ anisotropies that governs the (anti-)correlation between the kSZ and the EoR maps, the size of the ionized bubbles also play a key role. Recall that the average size of the ionization bubble is larger for 'QSOs'. As a result, the underlying structure within the ionized bubble will additionally reduce the anti-correlation and might change the scale of (anti-)correlation.

From now on we will just concentrate on cross-correlations using 'Stars' since the 'QSOs' model does not show a significant anti-correlation. Fig. 8 shows the correlation coefficient as a function of lag ($C(\theta)$) between the integrated kSZ and the integrated EoR map. The dashed red lines represents the estimated error obtained from Monte Carlo simulations. As in Salvaterra et al. (2005), we find that the two signals are anti-correlated below a characteristic angular scale θ_c and this scale indicates the average size of the ionized bubble which in our case is $\theta_c \approx 10$ arcmin.

Salvaterra et al. (2005) also showed that the amplitude of the anti-correlation signal increases with decreasing redshift and that the characteristic angular scale shows a redshift evolution. In order to test this in our simulation, we calculate the redshift evolution of the zero lag cross-correlation coefficient between the integrated kSZ map and the EoR map at different redshifts (Fig. 9). To calculate the error in the cross-correlation, we generate 200 different realizations of the kSZ and corresponding EoR cubes using the randomization procedure explained in Section 3. Then, around a desired redshift we fix the kSZ effect to zero and integrate along non-zero part of the kSZ cube. Finally, we cross-correlate the integrated kSZ map with the EoR map at the desired redshift and estimate the error on the cross-correlation between the integrated kSZ map and the EoR map at the certain redshift.

From Fig. 9, we find no coherent redshift evolution of the anti-correlation signal and on the contrary at few redshifts the two signals correlate instead of anti-correlating. The correlation at a given redshift is caused by i) the patchy nature of the EoR signal, which implies that there are some redshifts at which the EoR map contains none or only a few small ionized bubbles. If one correlates such an EoR map with the integrated kSZ map, the outcome is a correlation between the two, and because of an insignificant number of the ionization bubbles there is no contribution to the anti-correlation. ii) the kSZ signal being patchy. There are some redshifts where the kSZ signal from a certain ionization bubble does not contribute

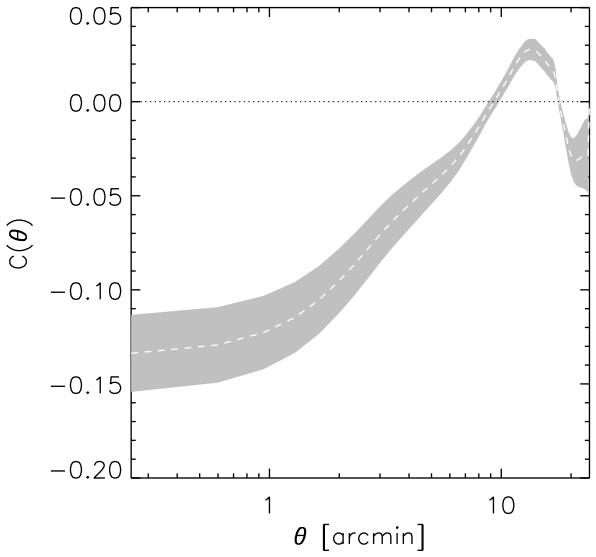

Figure 8. *The cross-correlation between integrated EoR and integrated kSZ map as a function of lag* ($C(\theta)$) *for the 'Stars' reionization history scenario (dashed white line). The gray shaded surface represents the estimated error obtained by Monte Carlo simulation. Note that the correlation coefficient at the zero lag is* $C_0 = -0.16 \pm 0.02$.

significantly or at all to the integrated kSZ map (see Fig. 10). This could happen due to a weak kSZ signal from a certain ionized bubble or due to cancellation of the kSZ signal from another ionization bubble along the LOS.

The analysis is repeated for different binnings in frequency of the EoR map but the results does not differ significantly. We also calculate the redshift evolution of the charateristic angular scale (θ_c), but we do not find any coherent evolution. This result is driven by the fact that the contribution of the kSZ signal from a certain redshift to the integrated kSZ map is not significant or is even non-existent. As a result, if there is no coherent redshift contribution to the integrated kSZ map there will be no coherent redshift evolution of the kSZ-EoR cross-correlation signal (see Fig. 10).

The discrepancy between our results and that of Salvaterra et al. (2005) is mainly due to the difference in the method to cal-

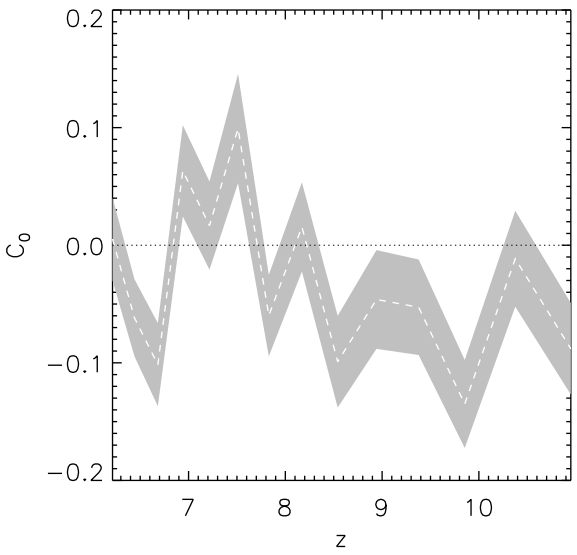

Figure 9. *The redshift evolution of the zero leg correlation coefficient between the integrated kSZ map and the EoR map at the certain redshift. The result is shown for the 'Stars' reionization history model. Note that the EoR map at the certain redshift is produced by integrating* $100\ h^{-1}$ Mpc *volume around the desired redshift.*

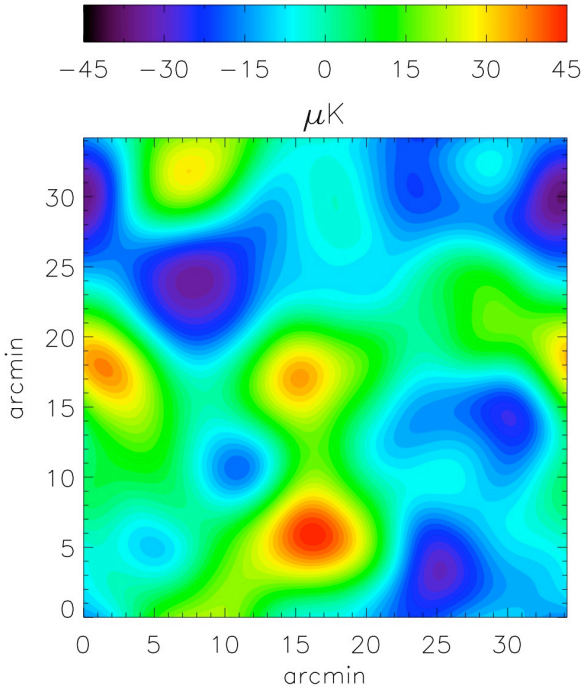

Figure 11. *The map of the primary CMB fluctuations generated as a Gaussian random filed with a power spectrum obtained from the CMBFAST algorithm.*

culate the cross-correlation coefficient. In Salvaterra et al., they first calculate the cross-correlation coefficient (not normalized) between a certain kSZ and EoR map. Then, they scramble both maps without keeping any structural information and calculate the cross-correlation coefficient. They compare the coefficients in the two cases to draw their conclusion. In contrast to Salvaterra et al., we first calculate the normalized cross-correlation coefficient (see Eq. 13) between a pair of kSZ-EoR map. And then for comparison, we preform a Monte Carlo simulation to generate different realizations of the kSZ and the EoR maps . However, despite the cross-correlation procedure used, once the primary CMB fluctuations are included we are not able to find any significant kSZ-EoR cross-correlation (see Sec. 4.4).

4.3 Large-scale velocity

Our simulation volume is $(100\ h^{-1}\ \mathrm{Mpc})^3$ (see Section 3). Thus, large-scale velocities associated with bulk motions, on scales $\gtrsim 100\ h^{-1}\ \mathrm{Mpc}$ are missing. The missing velocities represent $\sim 50\%$ of the total power in the velocity field as given by the linear theory.

Iliev et al. (2007) showed that the large-scale velocities on scales $\gtrsim 100\ h^{-1}\ \mathrm{Mpc}$ increases the kSZ signal. Motivated by this result, we approximately account for the missing large-scale velocities as follows: first, we assume that every $100\ h^{-1}\ \mathrm{Mpc}$ chunk of our simulation cube has a random large-scale velocity component v_{LS}. Since our simulation cube is produced using 15 simulation boxes ($100\ h^{-1}\ \mathrm{Mpc}$), we need in total 15 v_{LS}. We randomly choose a realization of the 15 v_{LS} based on a velocity field power spectra from linear theory. By doing this we ensure that the velocities are correlated at large scales. Finally we add the missing v_{LS} component to each $100\ h^{-1}\ \mathrm{Mpc}$ chunk of the simulated cube.

Based on 200 realizations of the large-scale velocity field, we have found that the large-scale velocities increase the kSZ signal during the EoR by 10%. But on average we do not find any significant increase or decrease in the kSZ-EoR cross-correlation. However, for $\sim$20% of all large-scale velocity realizations we find an increase in the cross-correlation signal by a factor two or larger and for $\sim$2% a factor three or larger.

4.4 Primary CMB

Up to now, in our cross-correlation analysis we only considered secondary CMB anisotropies generated by the kSZ effect. In the actual experiment, the CMB data will comprise not only the kSZ anisotropies which are secondary, but also the primary and other secondary CMB anisotropies (for a recent review see Aghanim et al. (2008)). In this subsection we will examine the influence of the primary CMB fluctuations on the detectability of the kSZ-EoR cross-correlation.

We simulate the primary CMB fluctuations in the following way: first the CMB power spectra is obtained using CMBFAST (U. Seljak & M. Zaldarriaga, 2003) and then the map of the primary anisotropy is produced as a random Gaussian field with this power spectrum. An example of the simulated primary CMB map is shown on the Fig. 11. The size of the map coresponds to the size of the simulated EoR and kSZ maps. Notice the leak in power at small scales due to Silk damping (Silk 1967).

In order to calculate the noise in the cross-correlation introduced by the primary CMB fluctuations, we generate 200 different realizations of the primary CMB (pCMB) fluctuations. We then add secondary kSZ anisotropies induced by the 'Stars' (map shown in the Fig. 7), and calculate the cross-correlation between the pCMB+kSZ map and the integrated cosmological 21 cm map. The obtained zero lag cross-correlation coefficient is 0.0 ± 0.3. The noise introduced by the primary CMB fluctuations is too large

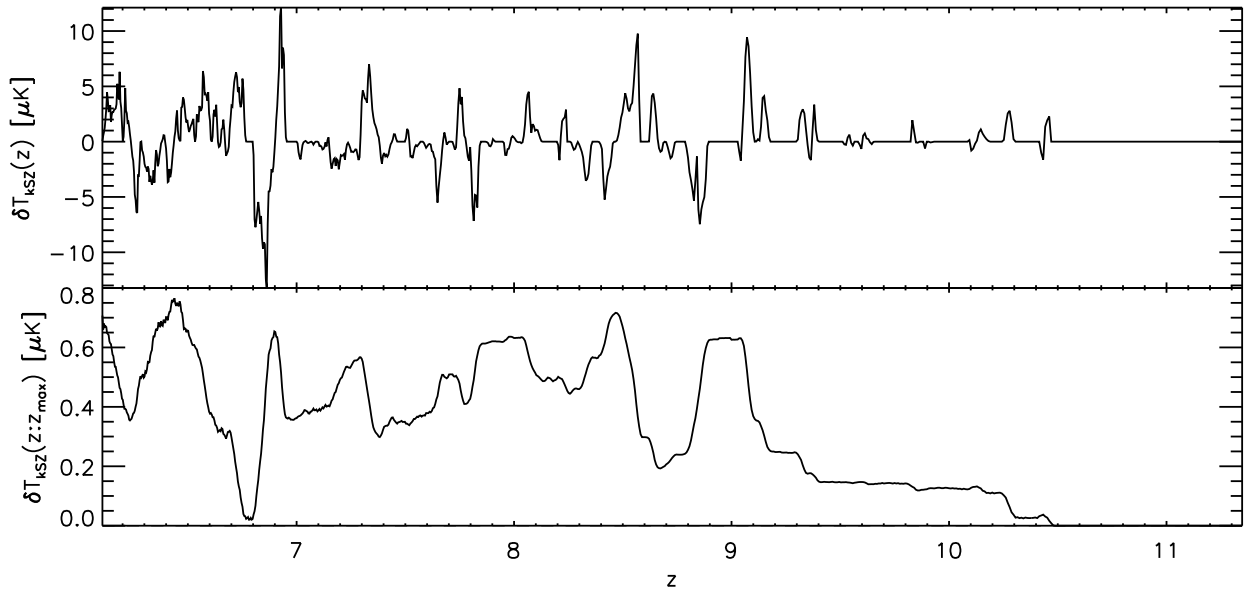

Figure 10. TOP PANEL: *A random line of sight through 'Stars' kSZ cube, $\delta T_{\rm kSZ}(z)$, that is averaged over 10 pixels (~ 0.7 arcmin) at each redshift.* BOTTOM PANEL: *For the same LOS the cumulative integral of the kSZ effect, $\int_{z_{\rm max}}^{z} \delta T_{\rm kSZ}(z){\rm d}z$. Note that there is no coherent redshift contribution to the integrated kSZ effect.*

to find any significant kSZ-EoR (anti-)correlation. However, one has to remember that the primary CMB anisotropies are damped on small angular scales and that on these scales the secondary anisotropies are the dominant component of the CMB power spectra (see Fig. 12). Utilizing this fact, one can do a cross power spectrum and see the correlation as a function of angular scale. Pursuing this lead, we calculate the kSZ-EoR cross spectrum first without and then with the primary CMB added to the kSZ map.

The cross spectrum ($C_l^{\rm X}$) between the two images of a small angular size is give by:

$$C_l^{\rm X} \simeq P_k^{\rm X} = \frac{1}{n_k} \sum_{p,q \in k} A_{p,q} \cdot B_{p,q}^{*}, \qquad (14)$$

where $A_{p,q}$ is Fourier transform of the first image, $B_{p,q}^{*}$ the complex conjugate of the Fourier transform of the second image and n_k is number of points in the k-th bin ($k = \sqrt{p^2+q^2}$). Note that we assume a 'flat-sky' approximation (e.g. White et al. 1999): $k^2 P(k) \simeq \frac{l(l+1)}{(2\pi)^2} C_l \mid_{l=2\pi k}$ which is valid for $l \gtrsim 60$.

Fig. 13 shows the cross power spectrum between the kSZ anisotropies and the integrated cosmological 21 cm map for reionization due to 'Stars'. It is evident from the plot that the two images anti-correlate on large scales ($l \lesssim 8000$) but that the anti-correlation becomes weaker towards the smaller angular scales. At angular scales $l \gtrsim 8000$, there is no (anti-)correlation.

We also calculate the cross power spectrum between integrated EoR map and integrated kSZ map with primary CMB fluctuations included. However, the noise introduced by the primary CMB is too large to find any significant correlation at scales $l \lesssim 8000$.

This result might be driven by the simulation box size and reionization scenarios considered in this study and does not mean that a cross-correlation signal is absent at all scales and reionization histories. In order to test this, one needs to explore the kSZ-EoR cross-correlation using simulation with the box size that is larger than the one used in this study ($100\ h^{-1}$ Mpc).

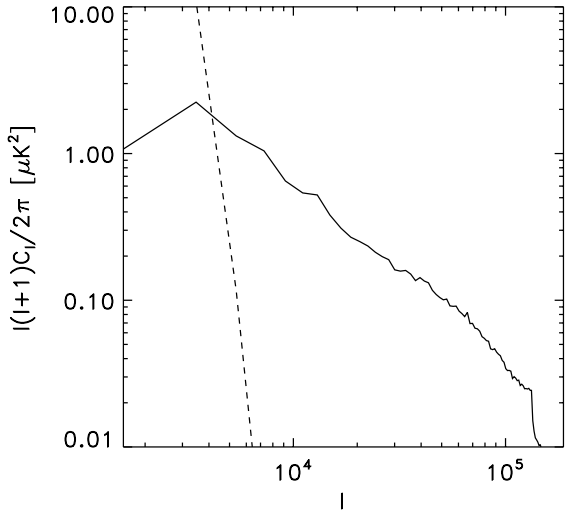

Figure 12. *The power spectra of primary CMB fluctuations (dotted line) and kSZ anisotropies obtained from the simulated maps (solid line).*

In the following subsection we try to use different cross-correlation methods and filtering techniques to explore the kSZ-EoR cross-correlation at scales where kSZ signal dominates over primary CMB fuctuations and where correlation signal is non-zero ($4000 \lesssim l \lesssim 8000$).

4.5 Additional cross-correlation techniques

For better understanding of the properties of the kSZ-EoR cross-correlation, and with the hope of being able to find the cross-correlation signal in the presence of primary CMB fluctuation, in this subsection we apply techniques of filtering, wavelet decompo-

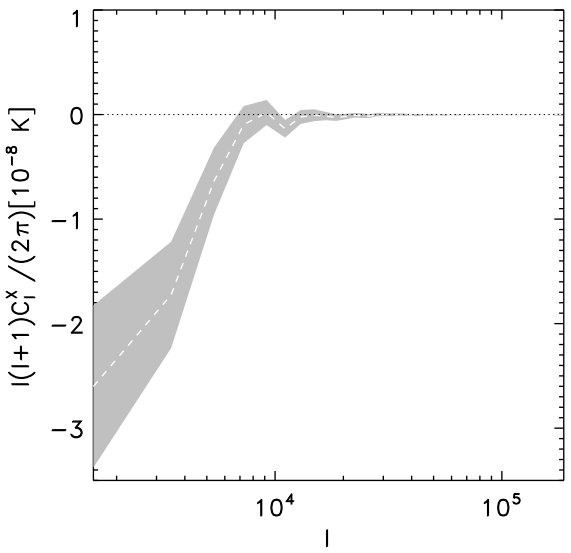

Figure 13. *The cross spectrum (see Eq. 14) between integrated kSZ map and integrated EoR map for the 'Stars' reionization history (dashed white line). The gray shaded surface represents the estimated error obtained by Monte Carlo simulation. Note that the primary CMB fluctuations are not included.*

sition and relative entropy on our data. We will only use the integrated kSZ map and integrated EoR map from the 'Stars' model of reionization, since the strongest cross-correlation signal is obtained for this model in the previous sections. Note that in a following analysis we first use only the kSZ and the EoR map and then as a second step we include the primary CMB fluctuations.

Fig. 14 shows the zero lag cross-correlation coefficient as a function of the three different filtering procedures. The first one uses a high-pass, the second a low-pass and the third a band-pass filter that passes out only a certain scale. In all three cases the filter is based on the 'Top hat' function. We filter out the desired scale from both the kSZ map and the EoR map and calculate the cross-correlation coefficient at zero lag. The results are shown for the low-pass and high-pass filter as a function of the FWHM of the filter and for the band-pass filter as a function of scale.

The plot on the left panel in Fig. 14 implies that the anti-correlation is strongest on the largest scales of the map. By adding smaller scales, the correlation coefficient decreases meaning that smaller scales introduce noise in the correlation. The middle panel in Fig. 14 suggests the same behaviour. By removing the large scales, the cross-correlation signal becomes quite small. Finally, the third panel of Fig. 14, suggests that the large scales are indeed the dominant component of the anti-correlation signal.

As a next step in our analysis we include the primary CMB fluctuations. However we obtain the same result as discussed in the previous subsection. On the scales where the kSZ anisotropies dominate over primary, or the anti-correlation signal is too weak or the noise introduced by residuals of the primary CMB fluctuations is too large to find any statistically significant kSZ-EoR (anti-)correlation.

The wavelet analysis of the maps is done using Daubechies and Coiflet wavelet functions. Both integrated kSZ map with added primary CMB flucutations and integrated EoR map are decomposed to a certain wavelet mode and then they are cross-correlated. Because the outcome is similar to that of filtering we will not discuss this further.

The last method applied to the data is the "relative entropy", also know as Kullback-Leibler distance. The relative entropy is a measure of the shared information between two variables (two images) by comparing the normalized distribution of the two. This method too did not produce any significant result.

5 DISCUSSION AND CONCLUSIONS

This paper presents a cross-correlation study between the kinetic Sunyaev-Zel'dovich (kSZ) effect and cosmological 21 cm signal produced during the epoch of reionization (EoR). The study uses an N-body/SPH simulation along with a 1-D radiative transfer code (the BEARS algorithm, Thomas et al. (2009)) to simulate the EoR and to obtain maps of the cosmological 21 cm signal and of the kSZ effect. The maps are produced using the $100\ h^{-1}$ Mpc comoving simulation box for five different (3 homogeneous and 2 patchy) models of reionization history. The homogeneous model with varying degree of "rapidness" of the reionization process is given by Eq. 12. The patchy reionization histories include one by 'Stars' (gradual) and the other by 'QSOs' (instant).

For a homogeneous reionization history we find that the kSZ map and the integrated EoR map are correlated. Furthermore, that the correlation depends on duration of reionization with larger values for more "rapid" models. This result agrees with the analytical kSZ-EoR cross-correlation analysis carried out by Alvarez et al. (2006).

For patchy reionization models we find that the kSZ temperature fluctuations are of the few μK level (see Table 1), and is in agreement with previously obtained results by Salvaterra et al. (2005); Iliev et al. (2007). In addition, we show that the temperature fluctuations induced by the patchiness of the reionization process ('δ_{x_e}' term in Eq. 4) is larger than the density induced fluctuations (homogeneous '$1+\delta$' term in Eq. 4). The difference between the two is stronger for the extended history ('Stars' model) than in more rapid reionization histories ('QSOs' model) (see Table 1).

As a first step in the kSZ-EoR cross-correlation study of patchy reionization histories we cross-correlate the kSZ map and EoR map at each redshift (see Fig. 1 & 2). As expected, the kSZ and the EoR map anti-correlate at certain redshifts (see Fig. 6).

We then cross-correlated the integrated cosmological 21 cm map and the integrated kSZ map for patchy reionization (see Fig. 7). The two signals show significant anti-correlation only in the 'Stars' model ($C_{0,\mathrm{Stars}} = -0.16 \pm 0.02$, $C_{0,\mathrm{QSOs}} = -0.05 \pm 0.02$.). The result is driven by the balance between homogeneous and patchy ('$1+\delta$' and 'δ_{x_e}' term in Eq. 4) kSZ anisotropies and the average size of the ionized bubbles. Since the homogeneous kSZ anisotropies correlate and patchy kSZ anisotropies anti-correlate with the cosmological 21 cm maps, the two effects tend to cancel each other. In addition the average size of the ionization bubble is larger for 'QSOs' than in 'Stars' model and the structure of matter within the ionized bubble reduce the cross-correlation. As a consequence the kSZ-EoR anti-correlation is much stronger for the extended ('Stars' model) reionization history than for a more instant history ('QSOs' model).

For a patchy model of reionization we estimated the redshift evolution of the correlation coefficient (C_0) and characteristic angular scale θ_{C}. This was done by cross-correlating the integrated kSZ maps with the EoR maps at different redshifts (see Fig. 9). In contrast to Salvaterra et al. (2005), we do not find any significant

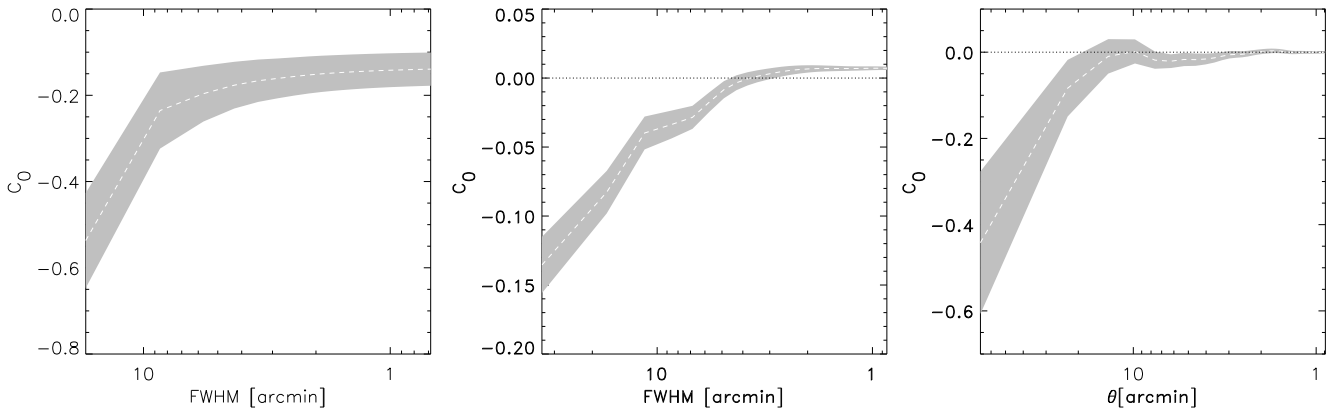

Figure 14. *The zero lag cross-correlation coefficient as a function of the three different filtering procedures. The first one uses a high-pass filter, the second one uses low-pass filter and the third a band-pass filter that passes only a certain scale. In all three cases the filter is based on the 'Top hat' function. The dashed white line is mean and the gray shaded surface represents the estimated error obtained by Monte Carlo simulation.*

coherent redshift evolution of C_0 and $\theta_{\rm C}$. The discrepancy between the results is caused by the difference in a procedure used for calculating cross-correlation. However, despite the cross-correlation procedure used, once the primary CMB fluctuations are included we are not able to find any significant kSZ-EoR cross-correlation.

The influence of the missing large-scale velocities on the kSZ signal and kSZ-EoR cross-correlation was investigated. Although, the large-scale velocities increase the kSZ signal by 10%, we do not find, on average, any significant change in the kSZ-EoR cross-correlation. However, for $\sim$20% of large-scale velocity realizations we find an increase in the cross-correlation signal by a factor two or larger and for $\sim$2% a factor three or larger.

Data from CMB experiments contains both the secondary (e.g. kSZ) and primary anisotropies. For completeness of our study we calculated the noise in the kSZ-EoR cross-correlation introduced by the primary CMB fluctuations and found that its addition reduces the cross-correlation signal to zero ($C_0 = 0.0 \pm 0.3$). The cross-correlation was also performed on scales where the kSZ anisotropies dominate over the primary CMB fluctuations ($l \gtrsim 4000$, see Fig. 12). We have done this by calculating cross-power spectra (Fig. 13), applying different filtering methods (Fig. 14) on the data and by doing wavelet decomposition. However, the outcome of the analysis is that on the scales where the kSZ anisotropies dominate over primary, or the anti-correlation signal is too weak or the noise introduced by residuals of the primary CMB fluctuations is too large to find any statistically significant kSZ-EoR (anti-)correlation.

As a sanity check we calculate the kSZ-EoR cross-correlation using the simulation obtained by Iliev et al. (2007) ('f250C' $100\ h^{-1}\ {\rm Mpc}$ simulation). The reionization history of this model is similar to our 'QSOs' model. The reionization history is relatively sharp and instant. The cross-correlation coefficient at zero lag for the integrated kSZ map and integrated EoR map is $C_0 = -0.04 \pm 0.02$. The result is in agreement with the result obtained from the 'QSOs' model. We also calculated the redshift evolution of the zero lag cross-correlation coefficient and have found no coherent redshift evolution.

In view of all the results obtained from the kSZ-EoR cross-correlation study, we conclude that the kSZ-EoR anti-correlation on scales captured by our simulation box ($\sim 0.6^\circ$) is not a reliable technique for probing the EoR. However, there is still hope that we will be able to find the correlation between the kSZ and EoR signal on scales larger than $\sim 1^\circ$, where the patchiness of the ionization bubbles should average out (see Alvarez et al. (2006) and Tashiro et al., *in preparation*). Finally, it is important to note that the kSZ signal induced during the EoR could still be detected in the power spectra of the CMB and used to place some additional constrains on this epoch in the history of our Universe.

ACKNOWLEDGEMENT

We acknowledge discussion with the LOFAR EoR key project members. The authors thank I. Iliev for providing us with Iliev et al. (2007) ('f250C' $100\ h^{-1}\ {\rm Mpc}$) simulation and A. Ferrara for useful comments. As LOFAR members VJ, SZ, LVEK and RMT are partly funded by the European Union, European Regional Development Fund, and by 'Samenwerkingsverband Noord-Nederland', EZ/KOMPAS.

REFERENCES

Adshead P. J., Furlanetto S. R., 2008, MNRAS, 384, 291
Aghanim N., Majumdar S., Silk J., 2008, Reports on Progress in Physics, 71, 066902
Alvarez M. A., Komatsu E., Doré O., Shapiro P. R., 2006, ApJ, 647, 840
Ciardi B., Madau P., 2003, ApJ, 596, 1
Cooray A., 2004, PhRvD, 70, 063509
Doré O., Holder G., Alvarez M., Iliev I. T., Mellema G., Pen U.-L., Shapiro P. R., 2007, PhRvD, 76, 043002
Dvorkin C., Hu W., Smith K. M., 2009, ArXiv e-prints
Fan X., Strauss M. A., Becker R. H., White R. L., Gunn J. E., Knapp G. R., Richards G. T., Schneider D. P., Brinkmann J., Fukugita M., 2006, AJ, 132, 117
Field G., 1958, Procedings of the IRE, 132, 240
Field G. B., 1959, ApJ, 129, 536
Furlanetto S. R., Zaldarriaga M., Hernquist L., 2004, ApJ, 613, 16
Gnedin N. Y., Jaffe A. H., 2001, ApJ, 551, 3
Gunn J. E., Peterson B. A., 1965, ApJ, 142, 1633
Harker G., Zaroubi S., Bernardi G., Brentjens M. A., de Bruyn A. G., Ciardi B., Jelic V., Koopmans L. V. E., Labropoulos

P., Mellema G., Offringa A., Pandey V. N., Schaye J., Thomas R. M., Yatawatta S., 2009a, ArXiv e-prints
Harker G. J. A., Zaroubi S., Thomas R. M., Jelić V., Labropoulos P., Mellema G., Iliev I. T., Bernardi G., Brentjens M. A., de Bruyn A. G., Ciardi B., Koopmans L. V. E., Pandey V. N., Pawlik A. H., Schaye J., Yatawatta S., 2009b, MNRAS, 393, 1449
Iliev I. T., Pen U.-L., Bond J. R., Mellema G., Shapiro P. R., 2007, ApJ, 660, 933
Jelić V., Zaroubi S., Labropoulos P., Thomas R. M., Bernardi G., Brentjens M. A., de Bruyn A. G., Ciardi B., Harker G., Koopmans L. V. E., Pandey V. N., Schaye J., Yatawatta S., 2008, MNRAS, 389, 1319
Komatsu E., Dunkley J., Nolta M. R., Bennett C. L., Gold B., Hinshaw G., Jarosik N., Larson D., Limon M., Page L., Spergel D. N., Halpern M., Hill R. S., Kogut A., Meyer S. S., Tucker G. S., Weiland J. L., Wollack E., Wright E. L., 2008, ArXiv e-prints
Labropoulos P., Koopmans L. V. E., Jelic V., Yatawatta S., Thomas R. M., Bernardi G., Brentjens M., de Bruyn G., Ciardi B., Harker G., Offringa A., Pandey V. N., Schaye J., Zaroubi S., 2009, ArXiv e-prints
Madau P., Meiksin A., Rees M. J., 1997, ApJ, 475, 429
Ostriker J. P., Vishniac E. T., 1986, ApJL, 306, L51
Page L., Hinshaw G., Komatsu E., Nolta M. R., Spergel D. N., Bennett C. L., Barnes C., Bean R., Doré O., Dunkley J., Halpern M., Hill R. S., Jarosik N., Kogut A., Limon M., Meyer S. S., Odegard N., Peiris H. V., Tucker G. S., Verde L., Weiland J. L., Wollack E., Wright E. L., 2007, ApJS, 170, 335
Salvaterra R., Ciardi B., Ferrara A., Baccigalupi C., 2005, MNRAS, 360, 1063
Santos M. G., Cooray A., Haiman Z., Knox L., Ma C.-P., 2003, ApJ, 598, 756
Silk J., 1967, Nature, 215, 1155
Slosar A., Cooray A., Silk J. I., 2007, MNRAS, 377, 168
Sunyaev R. A., Zeldovich Y. B., 1970, Astrophys. Space Sci., 7, 3
Tashiro H., Aghanim N., Langer M., Douspis M., Zaroubi S., 2008, MNRAS, 389, 469
Thomas R. M., Zaroubi S., 2008, MNRAS, 384, 1080
Thomas R. M., Zaroubi S., Ciardi B., Pawlik A. H., Labropoulos P., Jelić V., Bernardi G., Brentjens M. A., de Bruyn A. G., Harker G. J. A., Koopmans L. V. E., Mellema G., Pandey V. N., Schaye J., Yatawatta S., 2009, MNRAS, 393, 32
Vishniac E. T., 1987, ApJ, 322, 597
White M., Carlstrom J. E., Dragovan M., Holzapfel W. L., 1999, ApJ, 514, 12
Wouthuysen S. A., 1952, AJ, 57, 31
Zahn O., Zaldarriaga M., Hernquist L., McQuinn M., 2005, ApJ, 630, 657
Zaroubi S., Thomas R. M., Sugiyama N., Silk J., 2007, MNRAS, 375, 1269
Zeldovich Y. B., Sunyaev R. A., 1969, Astrophys. Space Sci., 4, 301
Zhang P., Pen U.-L., Trac H., 2004, MNRAS, 347, 1224

This paper has been typeset from a TEX/ LATEX file prepared by the author.